Iron/cobalt-SBA-16 cubic mesoporous composites as catalysts for the production of multi-walled carbon nanotubes

**D. Carta · F. Boi · A. Corrias · S. Bullita ·
Z. Kónya · M. F. Casula**

Abstract A series of catalysts containing iron and cobalt nanoparticles supported on a highly ordered mesoporous cubic *Im3m* silica (SBA-16) were prepared by wet impregnation and used for the production of multi-walled carbon nanotubes (MWCNTs) by catalytic chemical vapor deposition (CCVD) of acetylene. The catalysts were characterized by low- and wide-angle X-ray diffraction, N_2 physisorption analysis at 77 K and transmission electron microscopy to study the influence of different metal loading and impregnation time on the CCVD process. Quality and morphology of the MWCNTs was assessed by transmission and scanning electron microscopy, whereas thermal analysis was used to estimate the amount of CNTs produced. It was found that the nanocomposites are catalytically active with particular reference to samples with relatively high metal loading, and are stable under the conditions adopted for the CNT production by the CCVD process.

Keywords Mesoporous ordered materials · SBA-16 · Nanocomposites · Carbon nanotubes

D. Carta · F. Boi · A. Corrias · S. Bullita · M. F. Casula (✉)
Department of Chemical and Geological Sciences and INSTM, University of Cagliari, Cagliari, Italy
e-mail: casulaf@unica.it

Present Address:
A. Corrias
School of Physical Sciences, Ingram Building, University of Kent, Canterbury, UK

Z. Kónya
Department of Applied and Environmental Chemistry, University of Szeged, Szeged, Hungary

1 Introduction

Nanosized particles of transition metals and their bimetallic alloys (Fe, Co, Mn, Ni, Mo) have been extensively used in many heterogeneous catalytic reactions due to their small particle size and high surface to volume ratio. In particular, they have attracted much attention in recent years for their application as active sites for the catalytic production of carbon nanotubes (CNTs), which offer great promise as components in a variety of devices due to their peculiar electronic, mechanical, thermal and chemical properties [1, 2]. Methods that can be used for CNTs production include: arc-discharge, laser ablation, and catalytic chemical vapour deposition (CCVD). The latter, based on the catalytic thermal decomposition of light hydrocarbons (acetylene, ethylene, methane), has the advantage of relatively low operation temperatures (<1,000 °C), high yields, ease of scale-up, and leads to long, low-defect single- and multi-walled CNTs [3, 4].

The outcome of the CCVD process is highly dependent on the used catalyst, made out of nanophases based on transition metals dispersed in a thermally stable matrix. In particular, catalysts based on highly porous and high surface area matrix such as mesoporous ordered silicas are among the best candidates as support for nanoparticles to be used as catalysts for CNTs production [5]. Such porous silicas, exhibiting an ordered array of mesopores with uniform size, have been successfully applied in several fields of catalysis, including biocatalytic and environmental applications [6–8]. Concerning CNTs production, mesoporous silicas offer the advantage of having pore size in the range of typical CNTs diameters, and the uniform distribution of pore dimensions where nanoparticles are allocated facilitates the production of CNTs with a narrow distribution of diameters. In particular, a mesoporous

support with a 3D cage-like system of interconnected pores has the potential to be more efficient in catalysis compared to other common pore arrangements such as an hexagonal array formed by parallel pore channels that can be accessible only in one direction. Among the cubic mesoporous silicas, the so-called SBA-16, which has a porous structure with body-centred cubic symmetry (space group *Im3m*), is considered particularly interesting [9]. SBA-16 is formed by an arrangement of spherical empty cages where each cage is connected to eight neighbouring cages by narrow openings forming a 3D network of mesopores [10]. Thanks to the 3D cage-like cubic arrangement of mesopores, the high surface area and the thermal stability, SBA-16 appears to be an ideal material as catalytic support. In particular, the peculiar structure of SBA-16 should allow efficient transport of reactants through the interconnected network of mesopores.

In the present work, composites containing Fe and Co based nanoparticles dispersed in an ordered 3D cubic SBA-16 matrix have been prepared using the impregnation technique and used as catalysts for the production of CNTs. In particular, as iron and cobalt are among the most active metals towards the CCVD process and bimetallic catalysts have been reported to be more active compared to mono-metallic ones [11], iron–cobalt nanophases were dispersed on SBA-16 to obtain nanocomposites with enhanced catalytic activity towards the production of CNTs.

We investigate the effect of preparation conditions on the structural and textural features of the resulting porous nanocomposites by low angle and wide angle X-ray diffraction, transmission electron microscopy (TEM), and nitrogen physisorption techniques. The nanocomposites, based on an ordered mesoporous cubic silica support, are tested as catalyst for the production of multi-walled carbon nanotubes by a CCVD process. We demonstrate by characterization of the CCVD products through transmission and scanning electron microscopy, thermal analysis, and X-ray diffraction that multi-walled CNTs of high quality are obtained, with particular reference to porous nanocomposites with a relatively high loading of iron-cobalt nanophase.

2 Experimental section

Nanocomposites were prepared by wet impregnation of previously synthesized SBA-16. The synthesis of SBA-16 was performed according to ref. [12]. Pluronic F127 (P127, Aldrich) block copolymer, formed by a sequence of poly(ethylene oxide)-poly(propylene oxide)-poly(ethylene oxide) (EO_{106}-PO_{70}-EO_{106}) units with high molecular weight ($M_{av} = 12,600$) and high EO/PO ratio, was used as a structure directing agent. 4.0 g of P127 were added to a mixture of 30 g of water and 120 g of HCl 2 M under

stirring at room temperature. 8.5 g of TEOS (Aldrich 98 %) were then added to the solution which was left under stirring at room temperature for 20 h. The solution was aged for 2 days at 80 °C. The precipitate of SBA-16 was separated from the mother solution by centrifugation, washed with distilled water in order to remove H^+ and Cl^- ions and dried at room temperature. In order to remove the organic template (P127), the pure SBA-16 was then calcined by heating the product in air up to 500 °C with a heating step of 1 °C/min, and by keeping the final temperature of 500 °C for 6 h.

Nanocomposites were prepared by wet impregnation of 0.3 g of SBA-16 with 10 mL of an aqueous solution of $Fe(NO_3)_3 \cdot 9H_2O$ (Aldrich, 98 %) and $Co(NO_3)_2 \cdot 6H_2O$ (Aldrich, 98 %) and vigorously stirred. Different nanocomposites were prepared varying the total metal molar concentrations of Fe and Co ions (0.4 and 0.8 M) and impregnation time (1 and 24 h) while keeping the Fe:Co ratio equal to 2:1. The impregnated SBA-16 samples were separated from the solution by centrifugation. Afterwards, the impregnated SBA-16 samples were calcined in air at 500 °C, in order to transform the metal nitrates in metal oxides. The products calcined at 500 °C will be hereafter indicated as S_Z_Yh, where Z indicates the overall metal molar concentration and Y the stirring time.

CNTs were obtained by CCVD of acetylene (C_2H_2) at 750 °C over the Fe and Co based catalysts calcined at 500 °C. 100 mg of catalyst were placed in a quartz plate which was inserted into a reactor under a flow of 300 mL/min N_2 for 10 min. Then, the reactor was inserted into a furnace at 750 °C and N_2 was replaced with C_2H_2 (30 mL/min) which was fluxed for 20 min. Composites after CNTs productions will be named as S_Z_Yh_CNT.

The ordered mesoporous structure of the nanocomposites was studied by low-angle X-ray diffraction patterns recorded using Cu Kα radiation in transmission mode on a Panalytical Empyrean diffractometer equipped with a focusing mirror on the incident beam and an X'Celerator linear detector. The scans were collected within the range of 0.3°–3° (2θ) using a step size of 0.017°, 100 s per step. The same diffractometer was also used to record wide-angle X-ray diffraction (XRD) patterns. In this case, data were collected in Bragg–Brentano geometry with a graphite monochromator on the diffracted beam and the X'Celerator linear detector. The scans were collected within the range of 15°–85° (2θ).

Surface areas, pore sizes and pore volumes were obtained from N_2 adsorption–desorption measurements at 77 K recorded on a Sorptomatic 1990 System (Fisons Instrument). Surface area were estimated using the Brunauer–Emmett–Teller (BET) model, [13, 14] pore size and pore volumes were estimated using the Barret-Joyner-Halenda (BJH) method [15].

Table 1 Physical properties of catalysts as derived from physisorption data[a], TEM characterization[b], and ICP chemical analysis [c]

	Surface area[a] (m^2/g)	Pore volume[a] (cm^3/g)	Pore size[b] (nm)	Weight % Fe + Co[c]
S_0.4_1h	409	0.33	6.2	3.5
S_0.8_1h	358	0.28	5.5	6.1
S_0.4_24h	353	0.32	6.5	3.8
S_0.8_24h	470	0.61	6.2	7.7

Fig. 1 Wide angle XRD patterns of: (*a*) S_0.4_1h, (*b*) S_0.8_1h, (*c*) S_0.4_24h, (*d*) S_0.8_24h

Chemical composition was determined by inductively coupled plasma atomic emission spectrometry (ICP-AES) using a Varian Liberty 200 spectrophotometer. Solutions for the Fe and Co analysis content were prepared by dissolving about 20 mg of each nanocomposite in HF (Fluka, 40 %) and heating up until complete removal of tetrafluorosilicates. The residual solid was dissolved in a 250 mL volumetric flask using water and 10 mL of HNO$_3$ 1 M.
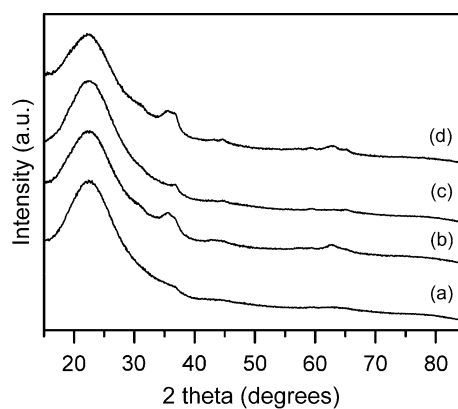
Thermal gravimetry (TG) and differential thermal analysis (DTA) were carried out using a Mettler-Toledo TG/SDTA 851 in the range 25–1,000 °C under oxygen flow (heating rate = 10 °C/min, flow rate = 50 mL/min).

Conventional transmission electron microscopy (TEM) images were recorded on a Jeol JEM 1011 Microscope, operating at 100 kV, equipped with a W thermionic electron source. Prior to observation the powdered samples were deposited on a carbon-coated copper grid.

Scanning Electron Microscopy (SEM) images were collected on a Hitachi S-4700 Microscope. Samples were placed on the surface of a piece of double-sided carbon adhesive tape which was attached to an aluminum sample holder.
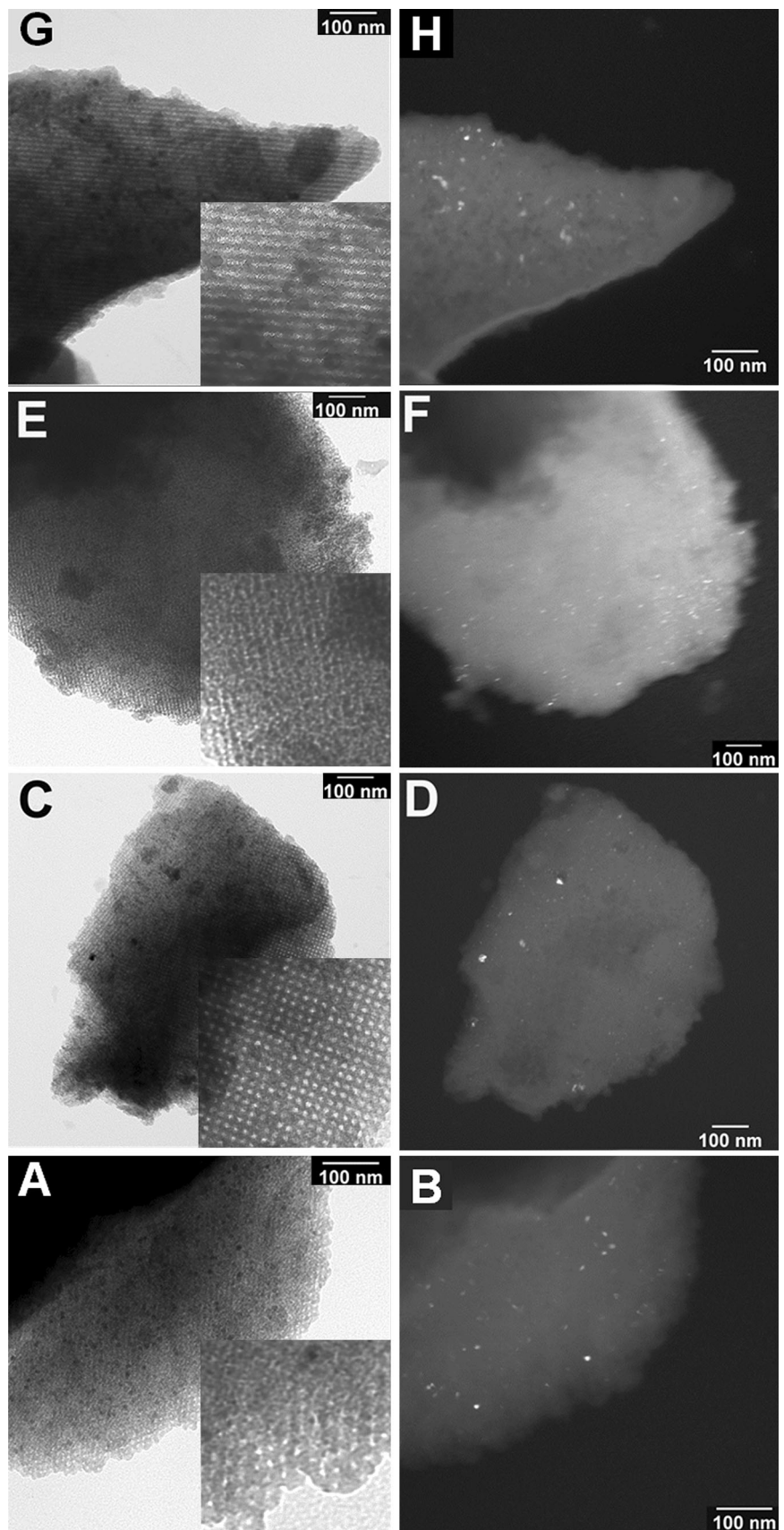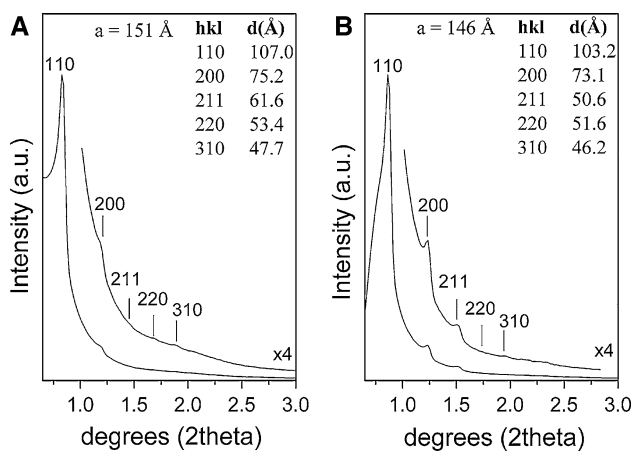
3 Results and discussion

Two sets of catalysts were prepared by impregnation of previously synthesized SBA-16 supports [12, 16] with Fe and Co ions solutions with the same Fe:Co ratio equal to 2:1 but varying the total metal molar concentrations (0.4 and 0.8 M). In both cases, the SBA-16 support was kept in contact with the solutions of the Fe and Co ions for either 1 or 24 h. The amount of Fe and Co measured by ICP analysis, was found to be 3.5 wt% in S_0.4_1h and 6.1 wt% in S_0.8_1h, clearly indicating that a higher loading can be achieved by using a more concentrated solution (Table 1). On the other hand, ICP analysis shows that impregnation time has a limited effect, since the total amount of Fe and Co increased only slightly to 3.8 wt% in S_0.4_24h and 7.7 wt% in S_0.8_24h, when the matrix was kept in contact with the solution for 24 h.
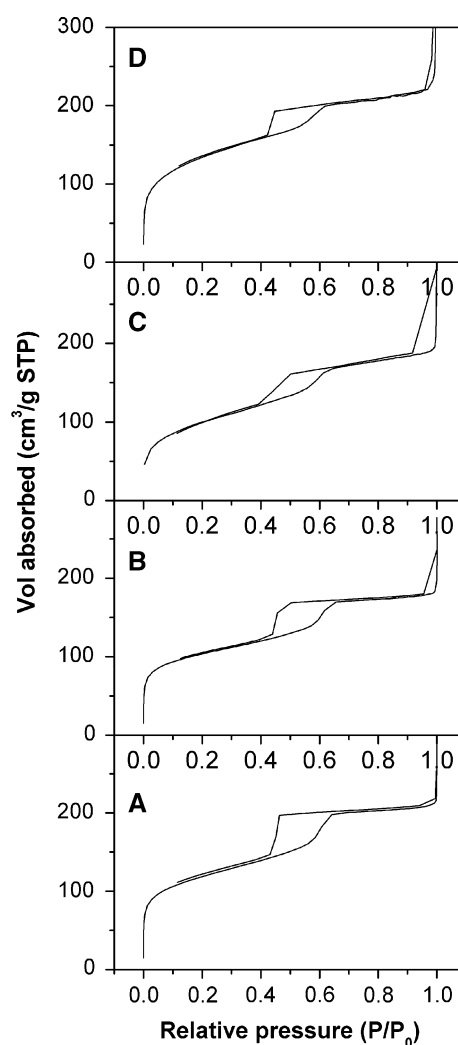
Fig. 2 N$_2$ adsorption–desorption isotherms at 77 K for: **a** S_0.4_1h, **b** S_0.8_1h, **c** S_0.4_24h, **d** S_0.8_24h

The peaks in the wide-angle XRD patterns of the catalysts, reported in Fig. 1, are broad and weak in all samples; however, they are more evident in the patterns of the more

Fig. 3 TEM images of: **a**, **b** S_0.4_1h, **c**, **d** S_0.8_1h, **e**, **f** S_0.4_24h, **g**, **h** S_0.8_24h. **a**, **c**, **e**, **g** bright field images (higher magnification images in the *insets*); **b**, **d**, **f**, **h** dark field images
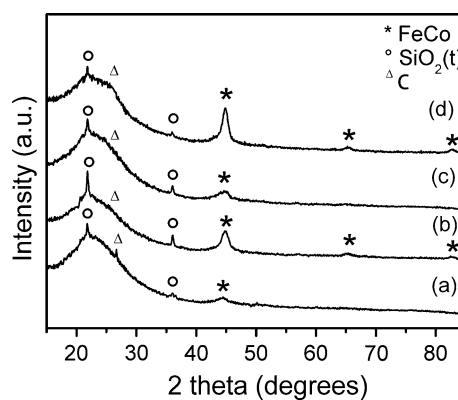
Fig. 4 Low-angle X-ray diffraction patterns of: **a** S_0.8_24h, **b** S_0.8_24h_CNT

Fig. 5 Wide angle XRD patterns of : (*a*) S_0.4_1h_CNT, (*b*) S_0.8_1h_CNT, (*c*) S_0.4_24h_CNT, (*d*) S_0.8_24h_CNT

concentrated S_0.8_1h and S_0.8_24h samples. Due to the nano dimensions of the dispersed phases and to the halo due to the amorphous silica matrix around $2\theta \sim 20°$–$30°$, phase identification is quite difficult. However, the observed reflections are consistent with the presence of Co_3O_4 (PDF card no. 42-1467) and to either 2-line ferrihydrite (F2L), or a spinel phase, such as γ-Fe_2O_3 (PDF card no. 39-1346) or $CoFe_2O_4$ (PDF card no. 22-1086). The weak peaks present in S_0.4_1h and S_0.4_24h samples are consistent with a spinel phase, taking into account our previous EXAFS study on the phases formed after calcination at 500 °C in similar SBA-16 systems [17].

The textural analysis of all the catalysts was performed using N_2 adsorption–desorption technique and the main textural parameters are reported in Table 1, whereas the isotherms of all the samples are shown in Fig. 2. They all show a type IV isotherm with a H2 hysteresis loop, which closes just above P/P_0 relative pressure of about 0.45, characteristic of ink-bottle mesopores, indicative of a cage-like cubic porous structure. Surface areas are all between 353 and 470 m²/g. Pore size values obtained by analysis of the adsorption branch are found to be around 5 nm for all samples.

The cubic cage-type mesoporous structure of all catalysts is also clearly visible in the TEM images, reported in Fig. 3. A highly ordered arrangement of mesopores which is consistent with a cubic mesostructure is evident in all samples. In order to show in detail the ordered mesoporous structure, higher magnification insets are shown for all samples. The images are taken along different directions and, in particular, the cubic arrangement of pores viewed along the [100] direction is evident in the inset of image C [18]. Pore diameter was estimated to be around 4 nm and wall thickness around 5 nm. It has to be noted that spherical nanoparticles (4–8 nm) homogeneously dispersed on

the SBA-16 support are clearly visible in the bright field images of all nanocomposites as dark spots. The presence of nanoparticles is even more evident in the dark field images (obtained using the first diffraction ring) where they appear as bright spots.

Further evidence of the cubic mesoporous structure was provided (see Fig. 4a for the S_0.8_24h nanocomposite) by low-angle XRD diffraction. A strong reflection corresponding to a d spacing of 107.0 Å and other reflections corresponding to d spacing of 75.5, 61.6, 53.4 and 47.7 Å, are detected. These reflections can be indexed as (110), (200), (211), (220) and (310) and ascribed to a body-centered cubic (bcc) *Im3m* symmetry. The unit cell parameter was calculated to be $a = 151$ Å.

It is well known that metal or alloy nanoparticles act as active sites for the production of CNTs. In a previous work, we have shown that in similar materials iron-cobalt alloy is formed when the composites are treated under reactive reducing atmosphere (800 °C for 2 h under H_2 flow) [18]. However it has been reported that better catalytic performances are obtained if the metals/alloys are generated in situ during the CNT production thanks to the hydrogen developed during the CCVD reaction [19, 20]. Taking this into account, the CCVD production of CNTs was performed on the samples calcined at 500 °C as catalyst, so that FeCo nanoparticles could be obtained by in situ reduction of the oxidized species present in these samples.

The XRD patterns of all samples after CNTs growth, shown in Fig. 5, give evidence of the formation of FeCo nanoparticles (PDF card 44-1433) during the CCVD reaction. As expected, FeCo reflections are more intense in the samples with the highest FeCo loading. The average size of the crystallite domains in the FeCo nanoparticles was estimated to be 12.3 nm in S_0.4_1h_CNT, 10.8 nm in S_0.8_1h_CNT, 6.3 nm in S_0.4_24h_CNT and 8.4 nm in S_0.8_24h_CNT. These values were determined using the Scherrer formula, $t = 0.91 \lambda/(B\cos\theta)$, where t is the

Fig. 6 TEM bright field images of: S_0.4_1h_CNT (**a**, **b**) S_0.8_1h_CNT (**c**, **d**) S_0.4_24h_CNT (**e**, **f**) S_0.8_24h_CNT (**g**, **h**)
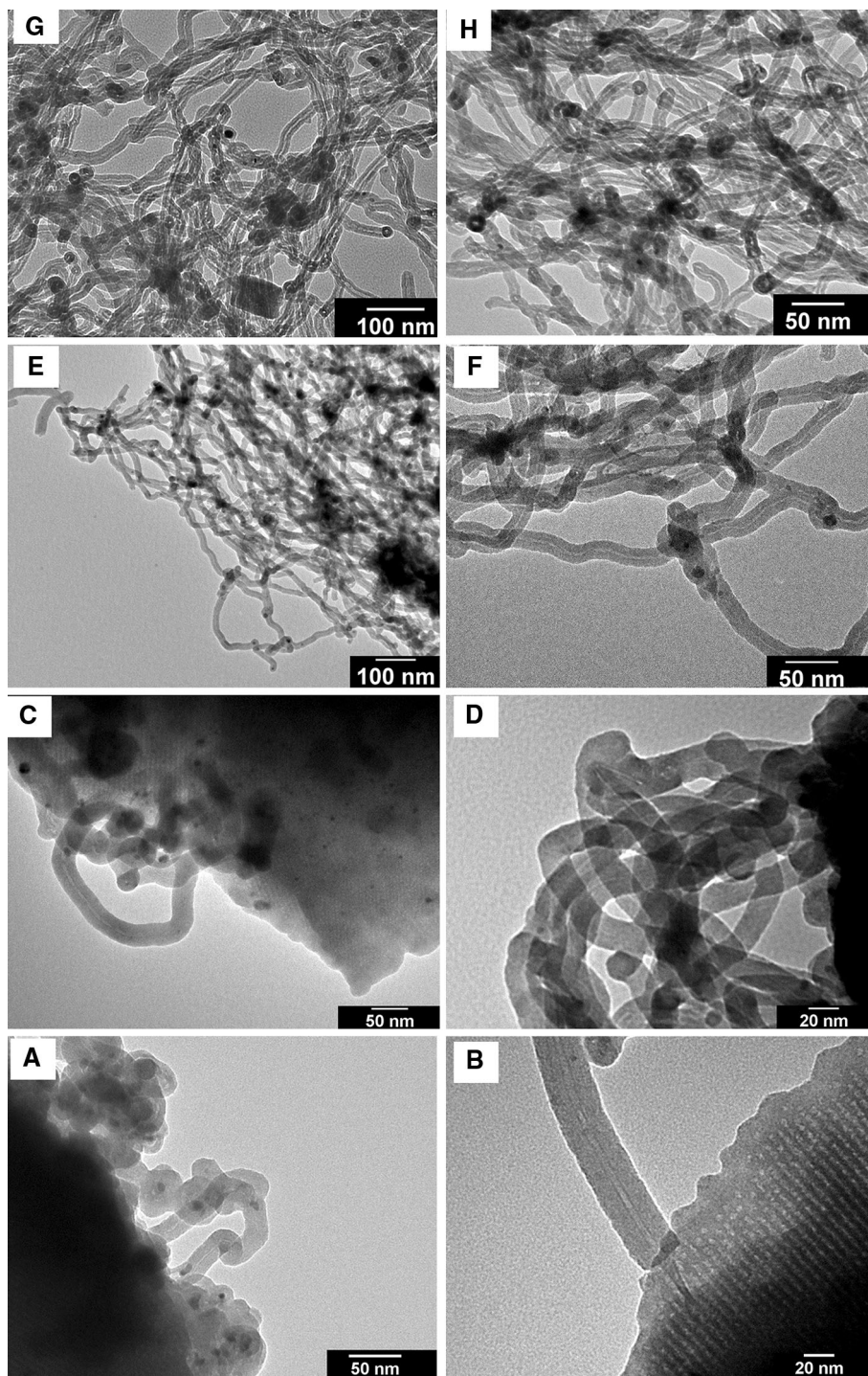

crystallite size, λ is the incident radiation wavelength, θ is the Bragg angle and B is the full-width at half-maximum of the diffraction peak (corrected for instrumental broadening). A reflection consistent with MWCNTs graphitic carbon (PDF card 41-1487) is observed in the region 2θ ∼ 25°–30°, as a shoulder in the broad halo at 2θ ∼ 20°–30° due to the amorphous silica matrix. Sharp peaks due to crystalline silica (trydimite, PDF card 42-1401) are also observed.

The TEM images shown in Fig. 6 provide evidence that CCVD gives rise to the formation of multi walled CNTs (MWCNTs) using all the catalysts. Additional information on the morphology of the MWCNTs is given by the SEM images, reported in Fig. 7.

Fig. 7 SEM images of:
a S_0.4_1h_CNT,
b S_0.8_1h_CNT,
c S_0.4_24h_CNT,
d S_0.8_24h_CNT
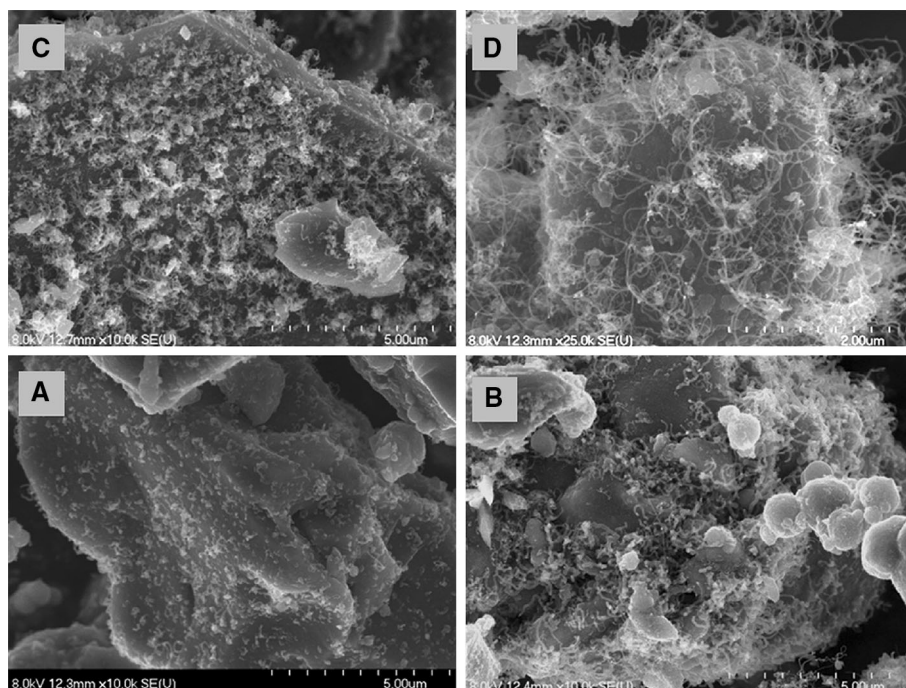
Round shaped FeCo nanoparticles can be observed in all the TEM images. From the statistical analysis of the FeCo nanoparticles sizes, carried out using around 25 nanoparticles, the average sizes were determined to be 11 ± 4, 8 ± 3, 6 ± 3, 10 ± 5 nm for S_0.4_1h, S_0.8_1h, S_0.4_24h and S_0.8_24h, respectively. It has to be noted that the average size of the crystallite domain determined from XRD is in agreement with the average FeCo nanoparticles dimensions determined by TEM.

An estimate of the outer and internal diameter and of the length of MCWTs was performed using statistical analysis. The MWCNTs produced using S_0.4_1h and S_0.8_1h are quite large, with an outer diameter of 29 ± 9 nm and 30 ± 4 nm and an inner diameter of 4 ± 3 and 3 ± 1 nm, respectively, as also confirmed by TEM images in Fig. 6a, b and c, d. The length of the MWCNTs was estimated to be 100 ± 36 nm for S_0.4_1h and 285 ± 153 nm for S_0.8_1h. SEM images (Fig. 7a, b) confirm that MWCNTs are relatively short and not very abundant.

The MWCNTs produced using S_0.4_24h and S_0.8_24h have an outer diameter of 17 ± 2 and 14 ± 6 nm and an inner diameter of 3 ± 1 and 5 ± 2 nm, respectively, as also shown in the TEM images reported in Fig. 6e, f and g, h. The length of MWCNTs produced using S_0.4_24h, estimated to be 351 ± 100 nm from statistical analysis, is in agreement with the length of MWCNTs observed in the SEM image reported in Fig. 7c where they appear relatively short. The SEM image of MWCNTs produced using S_0.8_24h, reported in Fig. 7d, shows longer MWCNTs than those produced using S_0.4_24h.

This is confirmed by the statistical calculation of the lengths that gives a value of 566 ± 125 nm for the latter. Regions of the ordered silica matrix together with the produced MWCNTs can be seen in Fig. 6b, c, indicating that the mesoporous periodic structure of the matrix is remarkably stable, as also confirmed by the low-angle XRD diffraction pattern of S_0.8_24h_CNT, reported in Fig. 2b, which shows that the mesoporous structure remained almost unchanged following the CCVD reaction, with just a slight contraction of the cubic lattice. The position of the main reflection corresponds to a d spacing of 103.2 Å (unit cell parameter of 146 Å), only slightly smaller than the value observed for the main reflection in S_0.8_24h.

In order to estimate the amount of produced CNTs, TGA and DTA measurements were performed on the catalysts after the CCVD process (Fig. 8). Two weight losses are observed in all samples: a first moderate weight loss between 25 and 150 °C (about 3–6 wt%), due to the loss of adsorbed water, and a second weight loss between 300 and 600 °C (about 20–25 wt%) corresponding to an exothermic event, as shown by the associated features in the DTA curves. In particular, DTA curves for S_0.4_1h_CNT (Fig. 8a) and S_0.4_24h_CNT (Fig. 8c) show a strong exothermic peak centred at about 400 °C and an additional weaker peak (marked by an arrow) at about 500 °C. The DTA curve of S_0.8_1h_CNT (Fig. 8b) shows some unresolved peaks in the region 450–600 °C and the DTA curve of S_0.8_24h_CNT (Fig. 8d) shows two prominent peaks, one centred at 450 °C and the other one at 550 °C.

Fig. 8 TG (*continuous line*) and DTA (*dotted line*) curves of S_0.4_1h_CNT (**a**) S_0.8_1h_CNT (**b**) S_0.4_24h_CNT (**c**) S_0.8_24h_CNT (**d**)
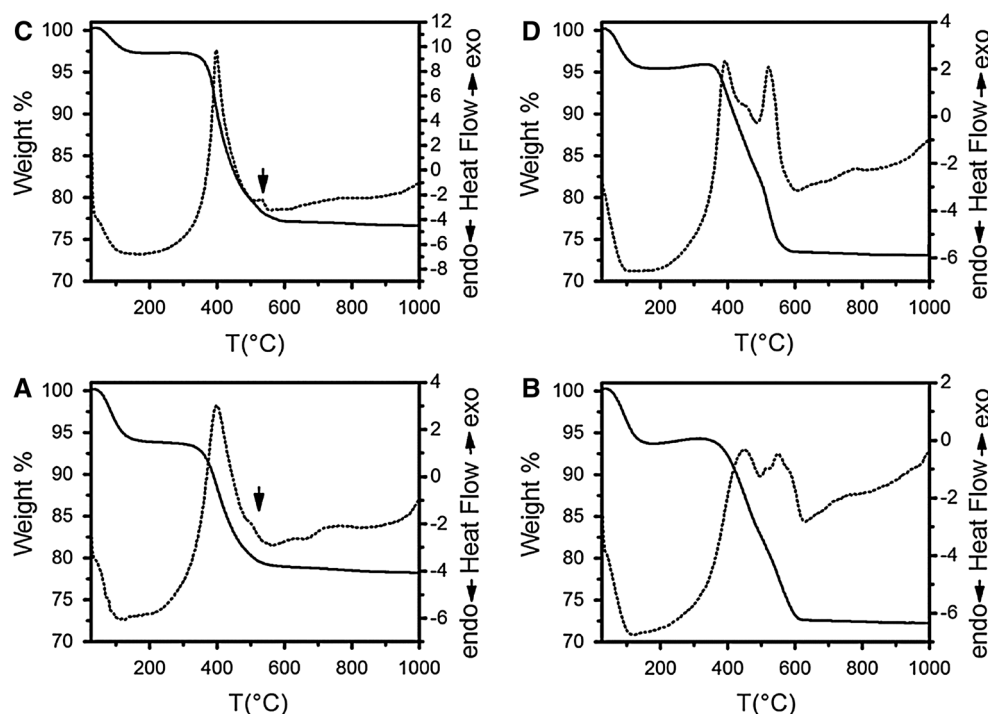
The features of the thermal analysis data can be used to support the data on the amount and quality of the carbon deposit formed upon the CCVD process, as it has been reported that thermal analysis of CNTs allows to distinguish amorphous carbon (which gives rise to a weight loss in the range 300–400 °C) from CNTs (which give rise to a weight loss at temperatures >400 °C) [21, 22]. On these basis, thermal analysis results suggest that a higher amount of CNTs is produced with the S_0.8_1h and S_0.8_24h nanocomposite catalysts than with S_0.4_1h_CNT and S_0.4_24h S_0.4_24h_CNT, in agreement with electron microscopy investigation. It should be pointed out, however, that caution must be taken in interpreting DTA results as oxidation temperature of CNTs depends on several parameters and the occurrence of catalytic metal particles embedded in the CNTs and defects may lower the thermal stability of CNTs [23].

4 Conclusions

We have prepared a series of high surface FeCo/SBA-16 porous nanocomposites where different loading of the metal nanophase was achieved by tuning the matrix impregnation conditions. The small size and high dispersion of the metal nanophase over the highly ordered cubic porous silica makes these nanocomposites suitable as catalysts for the CNT production through the CCVD process. The tested nanocomposites are catalytically active for the prduction of multi walled CNTs, the highest yield being achieved with S_0.8_1h and S_0.8_24h, likely due to the occurrence of a higher loading of metal nanophase in the catalyst. Transmission and scanning electron microscopy indicates that also the quality of the produced MWCNTs is improved in catalysts with highest metal loading. XRD analysis indicates that MWCNT production by the CCVD process involves the formation of FeCo alloy nanocrystals with size in the range 6–11 nm, dispersed into the mesoporous silica matrix. Remarkably, TEM and low-angle XRD diffraction show that the periodic cubic structure of the matrix is remarkably stable, and remains nearly unchanged following the CCVD reaction.

References

1. D. Vairavapandian, P. Vichchulada, M.D. Lay, Anal. Chim. Acta. **626**(2), 119 (2008)
2. J.M. Schnorr, T.M. Swager, Chem. Mater. **23**, 646 (2011)
3. K.Y. Tran, B. Heinrichs, J.-F. Colomer, J.-P. Pirard, S. Lambert, Appl. Catal. A. Gen. **318**, 63 (2007)
4. M. Kumar, Y. Ando, J. Nanosci. Nanotechnol. **10**(6), 3739 (2010)

5. J. Zhu, M. Yudasaka, S. Iijima, Chem. Phys. Lett. **380**, 496 (2003)
6. J. Ma, L. Li, J. Zou, Y. Kong, S. Komarneni, Microporous Mesoporous Mater. 193, 154 (2014)
7. J.M. Gomez, M.D. Romero, T.M. Fernandez, S. Garcia, J. Porous Mater. **17**, 657 (2010)
8. Z. Tan, A.A. Donaldson, Z. Zhang, J. Porous. Mater. **18**, 651 (2011)
9. E.M. Rivera-Muñoz, R. Huarache-Acuña, Int. J. Mol. Sci. **11**, 3069 (2010)
10. L. Li, D.L. King, J. Liu, Q. Huo, K. Zhu, C. Wang, M. Gerber, D. Stevens, Y. Wang, Chem. Mater. **21**, 5358 (2009)
11. E. Dervishi, Z. Li, Y. Xu, V. Saini, F. Watanabe, A.R. Biris, A. Bonpain, J.J. Garbay, A. Meriet, M. Richard, A.S. Biris, Particul. Sci. Technol. **27**, 222 (2009)
12. D. Zhao, Q. Huo, J. Feng, B.F. Chmelka, G.D. Stucky, J. Am. Chem. Soc. **120**, 6024 (1998)
13. S. Brunauer, P.H. Emmet, E. Teller, J. Am. Chem. Soc. **60**, 309 (1938)
14. F. Rouquerol, J. Rouquerol, K.S.W. Sing, Academic Press: London, (1999)
15. P. Barret, L.G. Joyner, P.P. Halenda, J. Amer. Chem. Soc. **73**, 373 (1951)
16. D. Carta, M.F. Casula, S. Bullita, A. Falqui, A. Corrias, J. Nanopart. Res. **13**, 3489 (2011)
17. D. Carta, G. Mountjoy, R. Apps, A. Corrias, J. Phys. Chem. C. **116**, 12353 (2012)
18. P. Ramesh, T. Okazaki, R. Taniguchi, J. Kimura, T. Sugai, K. Sato, Y. Ozeki, H. Shinohara, J. Phys. Chem. B. **109**, 1141 (2005)
19. D. Carta, S. Bullita, M.F. Casula, A. Falqui, A. Corrias, ChemPlusChem **78**, 364 (2013)
20. Y. Yang, Z. Hu, Y.N. Lu, Y. Chen, Mater. Chem. Phys. **82**, 440 (2003)
21. B.J. Landi, C.D. Cress, C.M. Evans, R.P. Raffaelle, Chem. Mater. **17**, 6819 (2005)
22. A. Falqui, D. Loche, M.F. Casula, A. Corrias, D. Gozzi, A. Latini, J. Nanosci. Nanotechnol. **11**, 2215 (2011)
23. S. Arepalli, P. Nikolaev, O. Gorelik, V.G. Hadjiev, W. Holmes, B. Files, L. Yowell, Carbon **42**, 1783 (2004)